

1 **Spatially repeatable components from ultrafast ultrasound are**  
2 **associated with motor unit activity in human isometric contractions**

3

4 Robin Rohlén<sup>1,2\*</sup>, Marco Carbonaro<sup>3,4\*</sup>, Giacinto L. Cerone<sup>3,4</sup>, Kristen M. Meiburger<sup>4,5</sup>, Alberto  
5 Botter<sup>3,4†</sup>, Christer Grönlund<sup>2†</sup>

6

7 1) Department of Biomedical Engineering, Lund University, Lund, Sweden

8 2) Department of Radiation Sciences, Radiation Physics, Biomedical Engineering, Umeå  
9 University, Umeå, Sweden

10 3) Laboratory for Engineering of the Neuromuscular System (LISiN), Department of  
11 Electronics and Telecommunication, Politecnico di Torino, Turin, Italy

12 4) PoliToBIOMed Lab, Politecnico di Torino, Turin, Italy

13 5) Biolab, Department of Electronics and Telecommunications, Politecnico di Torino, Turin,  
14 Italy.

15

16 \* These authors equally contributed to the work. Correspondence to Robin Rohlén or Marco  
17 Carbonaro. E-mail: [robin.rohlen@bme.lth.se](mailto:robin.rohlen@bme.lth.se), [marco.carbonaro@polito.it](mailto:marco.carbonaro@polito.it)

18

19 † These authors share senior authorship.

20

21 AB holds a patent on electrode technology for joint EMG and ultrasound acquisitions  
22 (WO2014009868A2). Other authors declare no competing interests.

23

## 24 **Abstract**

25 **Objective:** Ultrafast ultrasound imaging has been used to measure intramuscular mechanical  
26 dynamics associated with single motor unit (MU) activations. Detecting MU activity from  
27 ultrasound sequences requires decomposing a displacement velocity field into components  
28 consisting of spatial maps and temporal displacement signals. These components can be  
29 associated with putative MU activity or spurious movements (noise). The differentiation  
30 between putative MUs and noise has been accomplished by comparing the temporal  
31 displacement signals with MU firings obtained from needle EMG. Here, we examined whether  
32 the repeatability of the spatial maps over brief time intervals can serve as a criterion for  
33 distinguishing putative MUs from noise in low-force isometric contractions.

34 **Approach:** In five healthy subjects, ultrafast ultrasound images and high-density surface EMG  
35 (HDsEMG) were recorded simultaneously from biceps brachii. MUs identified through  
36 HDsEMG decomposition were used as a reference to assess the outcomes of the ultrasound-  
37 based decomposition. For each contraction, displacement velocity sequences from the same  
38 eight-second ultrasound recording were separated into consecutive two-second epochs and  
39 decomposed. The Jaccard Similarity Coefficient (JSC) was employed to evaluate the  
40 repeatability of components' spatial maps across epochs. Finally, the association between the  
41 ultrasound components and the MUs decomposed from HDsEMG was assessed.

42 **Main results:** All the MU-matched components had  $JSC > 0.38$ , indicating they were  
43 repeatable and accounted for about one-third of the HDsEMG-detected MUs ( $1.8 \pm 1.6$  matches  
44 over  $4.9 \pm 1.8$  MUs). The repeatable components (with JSC over the empirical threshold of  
45 0.38) represented 14% of the total components ( $6.5 \pm 3.3$  components). These findings align  
46 with our hypothesis that intra-sequence repeatability can differentiate putative MUs from  
47 spurious components and can be used for data reduction.

48 **Significance:** The results of our study provide the foundation for developing stand-alone  
49 methods to identify MU in ultrafast ultrasound sequences and represent a step forward towards  
50 real-time imaging of active MU territories. These methods are relevant for studying muscle  
51 neuromechanics and designing novel neural interfaces.

52

53 **Keywords:** motor unit, ultrafast ultrasound, electromyography, decomposition, territory

54

## 55 **Introduction**

56 Recently, neuromuscular imaging based on ultrafast ultrasound (UUS) has evolved  
57 considerably, opening new fronts in studying muscle contraction at the single motor unit (MU)  
58 level [1–9]. High-resolution imaging of active muscle tissue can provide spatiotemporal  
59 mechanics of individual MU fibres, complementing the information accessible with standard  
60 electrophysiological techniques for assessing single MU properties, i.e., invasive needle  
61 electromyography (nEMG) [10–12] and non-invasive surface EMG (sEMG) [13,14]. The  
62 added information on spatial and temporal mechanics can foster basic studies on muscle  
63 neuromechanics and force generation mechanisms [15], along with providing biomarkers for  
64 myopathic disorders [16–18], and innovative neural interfaces relevant, e.g., in rehabilitation  
65 and prosthetic control [19–21].

66

67 The methodology of identifying single MU activity in UUS recordings during isometric  
68 *voluntary* contractions was recently proposed based on a two-step approach [3]. First, the subtle  
69 intramuscular displacement velocities were estimated [22], and then these displacement  
70 velocities were decomposed into multiple components. Each component comprises a *spatial*  
71 map (location of the component, related to MU territory) and a *temporal* signal (time course of  
72 its displacement velocity, related to MU spike train). To separate spurious components (noise)

73 from those associated with single MU activation, a procedure based on *temporal* signal  
74 characteristics was adopted and later validated against single MU identification based on needle  
75 EMG [4]. It was found that a large proportion of the components' temporal twitch-by-twitch  
76 signals could not be matched with MU firings [4,6]. Two factors may contribute to this  
77 relatively low agreement between the two measures. The first is the heterogenic composition  
78 of linear and non-linear elastic tissue constituents, causing a non-linear combination of MU  
79 twitches. The second one concerns MU firing variability. Indeed, although the MU pool should  
80 be stable during these contractions, the firing rate of MUs varies, which has been shown to  
81 influence the temporal twitch parameters, i.e., alter the temporal signal (sequence of twitches)  
82 [15].

83  
84 In contrast to the temporal firing characteristics, the location of MU fibres within the muscle  
85 cross-section should represent an invariant feature during constant force and isometric  
86 contractions. It follows that components with a stable spatial map throughout the contraction  
87 are more likely to be associated with actual MU activations. Hence, we hypothesise that the  
88 spatial repeatability of a component across short epochs (intra-sequence repeatability) is a  
89 feature associated with MU activity and may be used as a criterion for data reduction of the  
90 initial decomposed components. In this study, we aimed to identify intra-sequence spatially  
91 repeatable components and examine whether repeatability can be used to separate MUs from  
92 noise in stable low-force isometric contractions. For this purpose, we decomposed displacement  
93 velocity images in consecutive two-second epochs from eight-second UUS recordings. We  
94 quantified the repeatability of the components' spatial map across epochs and examined  
95 whether the repeatable components were associated with actual MU activity. To this end, we  
96 used a set of reference MUs identified with an independent and validated decomposition  
97 method (HDsEMG decomposition [23]), applied to experimental signals detected

98 simultaneously with the ultrasound images. Finally, we determined whether the analysis based  
99 on two-second intervals (required to assess the repeatability) affects the number of MU-  
100 matched components compared with the decomposition of the recordings' full length (eight  
101 seconds).

102

## 103 **Methods**

### 104 **Experimental protocol**

105 Five subjects ( $31 \pm 6$  years, three males, and two females) performed three low-level isometric  
106 constant-force elbow flexions (from 2% to 10% of the maximum voluntary contraction). The  
107 details of the experimental protocol are reported in Carbonaro et al. [6]. Briefly, for each  
108 contraction, eight-second-long UUS recordings (Verasonics Vantage 128, Verasonics Inc.,  
109 Kirkland, WA) were recorded simultaneously [24] with HDsEMG (MEACS, LISiN,  
110 Politecnico di Torino, Turin, Italy [25]). A grid of 64 surface-EMG electrodes transparent to  
111 ultrasounds (8x8, 10 mm inter-electrode distance [26]) was placed on the muscle belly with the  
112 ultrasound transducer (L11-5v, 7.81 MHz centre frequency, 31.25 MHz sampling rate, and  
113 2500 Hz frame rate) positioned between the fourth and the fifth row of electrodes; i.e.  
114 transversally with respect to the muscle fibres' direction (Fig. 1A). The study was conducted  
115 following the Declaration of Helsinki and approved by the Regional Ethics Committee.  
116 Informed consent was obtained from all subjects.

117

### 118 **UUS and HDsEMG data processing**

119 The radio frequency UUS data comprised 20000 frames (2176x128 pixels, i.e., approximately  
120 53x40 mm). After traditional delay-and-sum beamforming, each eight-second dataset was  
121 processed in two-second epochs [3,4] with one-second overlapping ([0:2] s, [1:3] s, ..., [5:7] s,

122 [6:8] s) resulting in seven sub-datasets of two seconds (Fig. 1C). Each pixel in each sub-dataset  
123 was filtered over time with a 1D median filter with the order equal to 10 ms [3,4]. The image  
124 was cropped to 20x40 mm (850x128 pixels) [6,7] (Fig. 1D). For each epoch, displacement  
125 velocity images were calculated using 2D autocorrelation velocity tracking [22,27] with 1 mm  
126 in-depth and a sliding window of 10 ms (Fig. 1E). The temporal evolution of each pixel in the  
127 velocity images was high pass filtered at 3 Hz using 3<sup>rd</sup> order Butterworth filter (zero-phase) to  
128 attenuate slow movements not associated with muscle contraction [3]. Finally, the velocity  
129 images were down-sampled to 63x128 pixels, corresponding to approximately 0.3x0.3 mm per  
130 pixel.

131  
132 HDsEMG signals were bandpass filtered (20-400 Hz) and decomposed into individual MU  
133 spike trains [23] (Fig. 1K). The spike trains were edited [28] and resampled at the ultrasound  
134 frame rate. MU action potential (MUAP) amplitude distributions and their centroids were  
135 calculated using the longitudinal single differential MUAP decomposed from HDsEMG [29].  
136 Considering that the mediolateral surface covered by the HDsEMG grid is larger than that of  
137 the ultrasound transducer (Fig. 1A), all the centroids with the mediolateral coordinate outside  
138 the ultrasound field of view were truncated to the position of the first or last element of the  
139 probe (i.e., element 1 or 128).

140

#### 141 **Spatiotemporal decomposition of displacement velocity images**

142 As described in previous papers, the displacement velocity images were processed over five  
143 partially overlapping Region of Interest (ROIs) of 20x20 mm (5 mm increments) [4,6,8] (Fig.  
144 1F). We used spatiotemporal independent component analysis (stICA) [30] with  $\alpha = 1.0$  [8] to  
145 obtain 25 spatial components (*spatial maps*) and corresponding temporal components

146 (*temporal signals*) per ROI [4,8] (Fig. 1G). Hence, we obtained 125 spatiotemporal *ultrasound*  
147 *components* for each recording.

148

149 We clustered the intensities of each spatial map using the k-means algorithm with five clusters  
150 based on Euclidean distance (Fig. 1H). The cluster with the highest intensity values was  
151 assumed to be the localised spatial region (territory) of interest. Given this cluster, a binary map  
152 was generated. Objects with less than 25 connected pixels ( $\sim 1.5 \times 1.5 \text{ mm}^2$ ) were removed to  
153 remove noisy pixels at other regions in the image.

154

### 155 **Repeatability analysis: selecting similar spatial maps across epochs**

156 A Jaccard Similarity Coefficient (JSC) criterion based on the binary maps was used to select a  
157 set of similar spatial maps across different time epochs. Specifically, the 25 spatial maps of the  
158 *first two-second epoch* for each ROI were regarded as *reference* maps (Fig. 1I). Jaccard  
159 Similarity Coefficients were calculated between each *reference* map and the 25 maps obtained  
160 from each of the remaining six epochs. For each epoch, the map with the highest JSC was  
161 retained. This procedure provided, for each *reference* map, a selection of six spatial maps  
162 maximally similar to it. The *mean spatial map* and *mean JSC* (indicating the level of  
163 repeatability of a component) were then computed using the selected maps. In total, 25 mean  
164 spatial maps were identified for each of the five ROIs (125 mean spatial maps, including all  
165 five ROIs).

166

### 167 **Association of selected similar components with MUs from HDsEMG**

168 We studied the association between the ultrasound components selected in the previous  
169 paragraph and the characteristics of individual MUs identified through HDsEMG

170 decomposition. To this end, we considered the *temporal* signal corresponding to the selected  
171 spatial maps and the firing pattern of the MUs identified from HDsEMG.

172

173 The *temporal* signals of each set of selected components were spike-triggered averaged (Fig.  
174 1J) using the spike train of individual MUs identified from HDsEMG (Fig. 1K). This procedure  
175 was applied to all the combinations of selected ultrasound components and HDsEMG MUs,  
176 leading to a large set of *putative twitches* (Fig. 1J). Only those whose peak-to-peak amplitude  
177 exceeded a noise threshold were retained among these putative twitches. Among this subset,  
178 the pair (ultrasound component – HDsEMG MU) leading to the highest twitch amplitude was  
179 called the *MU-matched* component. The noise threshold was calculated by generating 125  
180 temporal components of coloured noise (5-30 Hz bandwidth of white noise) and spike-triggered  
181 averaged with 100 random spike trains (mean firing rates between 8-20 Hz and standard  
182 deviation of 15% of the mean inter-pulse interval [31]). The threshold value was computed as  
183 the mean plus two standard deviations of the peak-to-peak amplitudes of all the combinations  
184 of random components and spike trains.

185

### 186 **Number of matched components with MUs from HDsEMG: intra and full sequence** 187 **approach**

188 We intended to assess whether the analysis on two-second intervals, required to assess the  
189 repeatability, affected the number of MU-matched components. Therefore, we compared the  
190 number of MU-matched components found with the *intra-sequence* repeatability approach with  
191 the components decomposed from the stICA applied over the *full sequence recording* [4]. In  
192 both approaches, the matching with HDsEMG MUs was performed using the same method  
193 described in the previous paragraph.

194



## 195 **Statistical analysis**

196 We calculated descriptive statistics associated with the components (epochs and full sequence)  
197 and the MUs decomposed from HDsEMG. Based on the matched components with MU, we  
198 calculated the area, equivalent diameter (square root of  $4 \times \text{Area} / \pi$  as in [3]), and depth of the  
199 centroid of the component below the skin. In addition, the distance between the mediolateral  
200 centroids of the spatial map (based on the binary map) and MUAP spatial distribution (based  
201 on the spike-triggered average on the HDsEMG signals using the MU spike trains [29]) for  
202 each matched component and MU was calculated.

203

204 We tested the pairwise difference between the number of MU-matched components between  
205 the intra-sequence repeatability and the full sequence approach using a two-sided Wilcoxon  
206 signed rank test. In addition, we tested the difference in median JSC and normalised peak-to-  
207 peak amplitude, respectively, between the MU- and non-MU-matched components using the  
208 Mann-Whitney U test. The significance level was set to 0.05.

209

## 210 **Results**

211 Out of 20 recordings, 99 MUs ( $4.9 \pm 1.8$  MUs per recording) were identified by decomposing  
212 HDsEMG signals. The MUs had stable spike trains over the eight-second recordings with firing  
213 rates of  $12.3 \pm 2.1$  Hz.

214

215 We observed various degrees of intra-sequence repeatability across the 125 ultrasound  
216 components per recording, as shown by the large variability of JSC values (Fig. S1 in  
217 Supplementary material). Fig. 2 depicts two examples of repeatable components (high mean  
218 JSC) and one non-repeatable component (low mean JSC) from one ROI of a representative  
219 subject recording.

220

## 221 **Association of selected similar components with MUs from HDsEMG**

222 The scatterplot of Fig. 3 shows the relationship between JSC values and the amplitude of the  
223 (spike-triggered averaged) *putative twitches* from all subjects and trials. Each data point in Fig.  
224 3 represents an ultrasound component and an HDsEMG MU that provided the *putative twitch*  
225 with the highest amplitude. Those below the noise thresholds (grey dots in Fig. 3) were  
226 discarded among these data points. In some instances, the above threshold *putative twitches*  
227 (coloured dots in Fig. 3) was obtained by combining the same MU and different ultrasound  
228 components. In these cases, the combination leading to the highest *putative twitch* was retained  
229 (*MU-matched* components, red circles in Fig. 3). The *MU-matched* components had a higher  
230 JSC than the *non-MU-matched* (grey dots) components ( $0.61 \pm 0.12$  vs  $0.26 \pm 0.26$ ;  $p < 0.001$ )  
231 (Fig. 3). Noteworthy, the *MU-matched* components had a mean JSC always greater than 0.38,  
232 suggesting good repeatability (Fig. 2). In addition, defining the components as *repeatable* using  
233 this empirical threshold of 0.38, each recording had  $6.5 \pm 3.3$  repeatable components.

234

235 Fig. 4 shows three representative examples illustrating the spatial agreement between MUAP  
236 distributions and spatial maps of the *MU-matched* components together with the corresponding  
237 velocity twitches obtained with spike trigger averaging over all the MU firings of all epochs.  
238 *MU-matched* components were spatially (medio-laterally) adjacent to the MUAP distribution  
239 (Table 1), as demonstrated by the mediolateral distance between the centroid of the MUAP  
240 distributions and the centroid of the spatial maps ( $5.35 \pm 5.17$  mm,  $N = 35$  MU). The centroids  
241 of the mean spatial maps were distributed across the whole field of view with depths between  
242 2.90 mm and 14.01 mm (Table 1). In addition, the *MU-matched* components had a diameter of  
243  $4.03 \pm 1.28$  mm, similar to previously reported findings of MU territory size using scanning-  
244 EMG [32].

245

246 **Number of matched components with MUs from HDsEMG: intra and full sequence**

247 **approach**

248 The intra-sequence analysis led to 35 *MU-matched* components, i.e., 35.4% of the MUs  
249 identified by HDsEMG (Table S1, Supplementary material). By decomposing the full eight-  
250 second UUS, we found 36 matches, i.e., 36.4% of the MUs identified by HDsEMG. We found  
251 no difference in the number of matched MUs across all recordings concerning the two  
252 approaches ( $p = 0.9844$ ).

253

## 254 **Discussion**

255 This study investigated whether the spatial repeatability of components extracted from UUS  
256 sequences can be used as a criterion to separate muscle tissue displacements associated with  
257 single MU activation from noise during stable low-force isometric contractions. First, we  
258 decomposed displacement velocity sequences from consecutive two-second epochs of eight-  
259 second UUS recordings. Then, we quantified the repeatability of the components' spatial map  
260 across epochs and examined whether there was an association between the repeatability level  
261 and the degree of matching with reference MUs identified through HDsEMG decomposition.  
262 Finally, we investigated whether this intra-sequence approach using short epochs affects the  
263 number of matched MUs by comparing it with the decomposition of the recordings' full length  
264 (eight seconds). We obtained three main findings: 1) all the MU-matched components had a  
265 JSC larger than 0.38 and accounted for about one-third of the HDsEMG-detected MU, (2) The  
266 components with  $JSC > 0.38$  represented approximately 14% of the 125 initial components  
267 from each recording, and (3) the number of MU-component matches did not differ between the  
268 intra- and full-sequence approaches.

269

270 About 14% of the spatiotemporal components identified applying stICA to UUS sequences  
271 were matched with MUs decomposed independently from HDsEMG. A common characteristic  
272 of all the *MU-matched* components was the high JSC (Fig. 3) of their spatial maps. This  
273 evidence suggests that spatial repeatability across a short epoch is a relevant feature useful to  
274 identify putative MUs and implement data reduction methods on the initial set of ultrasound  
275 components. This result confirms the initial hypothesis, i.e., since the location of the MU fibres  
276 is an invariant feature of the MU during stable isometric contractions, *repeatable* spatial maps  
277 are more likely to be associated with actual MUs. Whether this hypothesis applies to conditions  
278 other than isometric or constant force contractions likely depends on how MU territory is  
279 represented in the ultrasound scanning plane and how this representation changes during a  
280 contraction. For instance, muscle shape changes occurring during dynamic contractions may  
281 lead to a shift or a shape change of the area where MU fibres' activation induces movement  
282 within the muscle cross-section, i.e., within the ultrasound scanning plane. This would clearly  
283 undermine the assumption of MU territory spatial invariance, which is the basis for our  
284 hypothesis. Although to a lesser extent, similar variations in MU territory representation can  
285 also occur during isometric contractions, for instance, during force-varying contractions,  
286 fatiguing contractions or any condition inducing a progressive MU recruitment or de-  
287 recruitment. Further studies are required to quantify the effects of these factors on UUS  
288 decomposition.

289  
290 About one-third of MUs decomposed from HDsEMG matched with repeatable ultrasound  
291 components. This is similar to the number of successful identifications found in previous  
292 studies. It has been previously associated with differences in detection volume and  
293 characteristics of two detection systems (EMG and ultrasound) [4,6,33]. In addition to the  
294 characteristics of the two measuring techniques, it is worth noting that the measured system is

295 expected to be non-linear due to the heterogenic composition of linear and non-linear elastic  
296 constituents. Already at 5-10% MVC, many MUs are active and may suppress or distort the  
297 triggered twitch amplitude. Another aspect to consider is that, in this study, we found more  
298 repeatable ultrasound components for each recording ( $6.5 \pm 3.3$ ) than HDsEMG MUs ( $4.9 \pm$   
299  $1.8$ ). Although ultrasound provides a larger field of view and higher spatial resolution than  
300 HDsEMG, it remains unclear whether these unmatched repeatable components are MUs and  
301 whether they identify different MUs in the whole active MU population. In the present study,  
302 the number of successful identifications may have been biased by one subject for which our  
303 matching criteria led to no matched MUs. This case was most likely due to the poor quality of  
304 the displacement velocity images. The exclusion of this subject would have increased the  
305 percentage of MU-matches from 35.4% to 42.7% for the intra-sequence repeatability approach  
306 and from 36.4% to 43.9% for the original decomposition over the full sequence (Table S1,  
307 Supplementary Material).

308  
309 Decomposing displacement velocity images into components using stICA over partially  
310 overlapping windows likely resulted in component duplicates. Fig. 5a shows two examples of  
311 duplicates in which three different components decomposed in three consecutive ROIs showed  
312 an amplitude of the twitches (related to the same MU firings) over the noise threshold. In this  
313 case, the component providing the highest twitch amplitude was selected and regarded as the  
314 MU-matched component. Moreover, it is worth noting that the stICA approach we used  
315 assumes spatial independence to decompose the dataset [30,34]. For this reason, it may split  
316 MU territories into separate components if the MU activation results in complex movements,  
317 e.g. due to the interaction between active and passive tissue [35,36] or tissue rotation due to so-  
318 called MU twisting [1,7]. In this regard, Fig. 5b shows two examples of MU twisting of two  
319 identified MUs. Two components (matched with the same MU) are spatially separated in two

320 regions of activation (blue and green spots in Fig. 5b) close to each other with inverted twitch  
321 shapes (blue and green twitches in Fig. 5b). The shape of the twitch is related to the direction  
322 of the movement. In Fig. 5b, the green twitches are negative (i.e., towards the probe/up), while  
323 the blue ones are positive (i.e., away from the probe/down). All these examples of duplicate  
324 components are now separated and contribute to the above-threshold components in Fig. 3  
325 (small orange points). In future studies, components belonging to the same MU may be merged  
326 considering the spatial overlay or a correlation approach based on, e.g., the temporal signals.

327

328 Although finding repeatable components requires eight seconds with the intra-sequence  
329 approach herein proposed, the results of this study confirm previous studies that the UUS  
330 decomposition method can identify possible MU activity in recordings as short as two seconds  
331 [4]. Identifying MUs from a short sequence is an advantage over other methods, such as spike-  
332 triggered averaging [9], which requires longer recordings due to other simultaneously active  
333 MUs and the motion of non-muscular structures hiding large parts of the movement caused by  
334 the target MU. Therefore, the blind source separation approach provides advantages compared  
335 to the spike-trigger averaging approach, such as lower memory and storage requirements and a  
336 potential to be used for, e.g., real-time imaging [37] and dynamic contractions applications. For  
337 these applications, future studies must consider the lower bound in terms of the recording  
338 duration to identify MUs and improve the classification of components into MUs or non-MUs  
339 using robust features or training a classifier. For example, the Gaussian-like 2D distribution of  
340 velocities reported in this work for the most repeatable components and similar to what has  
341 been found in previous studies [1,4,6,7], may be a feature for the classification of a component  
342 as a MU. Thus, having a classifier for MU/non-MU-associated components enables the UUS  
343 approach to be stand-alone from HDsEMG.

344

345 In conclusion, this study investigated the association of intra-sequence repeatable components  
346 with individual MU activity. We found that 1) spatial repeatability can be used as a data  
347 reduction to select putative MU activity during stable isometric contractions, and 2) the UUS  
348 decomposition method can identify possible MU activity in two-second recordings equally well  
349 as in eight-second recordings. These findings provide a foundation for developing stand-alone  
350 methods to identify MU in ultrafast ultrasound and represent a step towards real-time imaging  
351 of active MU territories.

## 352 **References**

- 353 [1] Deffieux T, Gennisson J L, Tanter M and Fink M 2008 Assessment of the  
354 mechanical properties of the musculoskeletal system using 2-D and 3-D very high frame rate  
355 ultrasound *IEEE Transactions on Ultrasonics, Ferroelectrics, and Frequency Control* 2177–  
356 90
- 357 [2] Grönlund C, Claesson K and Holtermann A 2013 Imaging two-dimensional  
358 mechanical waves of skeletal muscle contraction *Ultrasound in Medicine and Biology* **39** 360–  
359 9
- 360 [3] Rohlén R, Stålberg E, Stöverud K H, Yu J and Grönlund C 2020 A Method for  
361 Identification of Mechanical Response of Motor Units in Skeletal Muscle Voluntary  
362 Contractions Using Ultrafast Ultrasound Imaging - Simulations and Experimental Tests *IEEE*  
363 *Access* **8** 50299–311
- 364 [4] Rohlén R, Stålberg E and Grönlund C 2020 Identification of single motor units  
365 in skeletal muscle under low force isometric voluntary contractions using ultrafast ultrasound  
366 *Scientific Reports* **10** 1–11
- 367 [5] Ali H, Umander J, Rohlén R and Grönlund C 2020 A deep learning pipeline for  
368 identification of motor units in musculoskeletal ultrasound *IEEE Access* **8** 170595–608
- 369 [6] Carbonaro M, Meiburger K M, Seoni S, Hodson-Tole E F, Vieira T and Botter  
370 A 2022 Physical and electrophysiological motor unit characteristics are revealed with  
371 simultaneous high-density electromyography and ultrafast ultrasound imaging *Scientific*  
372 *Reports* **12** 1–14
- 373 [7] Lubel E, Grandi-Sgambato B, Barsakcioglu D Y, Ibanez J, Tang M-X and Farina  
374 D 2022 Kinematics of individual muscle units in natural contractions measured in vivo using  
375 ultrafast ultrasound *Journal of Neural Engineering* **19** 056005
- 376 [8] Rohlén R, Yu J and Grönlund C 2022 Comparison of decomposition algorithms



- 377 for identification of single motor units in ultrafast ultrasound image sequences of low force  
378 voluntary skeletal muscle contractions *BMC Research Notes* **15** 207
- 379 [9] Carbonaro M, Zaccardi S, Seoni S, Meiburger K M and Botter A 2022 Detecting  
380 anatomical characteristics of single motor units by combining high density electromyography  
381 and ultrafast ultrasound: a simulation study *2022 44th Annual International Conference of the*  
382 *IEEE Engineering in Medicine & Biology Society (EMBC)* (IEEE) pp 748–51
- 383 [10] Adrian E D and Bronk D W 1929 The discharge of impulses in motor nerve  
384 fibres: Part II. The frequency of discharge in reflex and voluntary contractions *The Journal of*  
385 *physiology* **67** 9–151
- 386 [11] Stålberg E and Antoni L 1980 Electrophysiological cross section of the motor  
387 unit. *Journal of Neurology, Neurosurgery and Psychiatry* **43** 469–74
- 388 [12] Daube J R and Rubin D I 2009 Needle electromyography *Muscle & Nerve:*  
389 *Official Journal of the American Association of Electrodiagnostic Medicine* **39** 244–70
- 390 [13] Fuglevand A J, Winter D A, Patla A E and Stashuk D 1992 Detection of motor  
391 unit action potentials with surface electrodes: influence of electrode size and spacing *Biological*  
392 *Cybernetics* **67** 143–53
- 393 [14] Farina D, Merletti R and Enoka R M 2014 The extraction of neural strategies  
394 from the surface EMG: an update *Journal of Applied Physiology* **117** 1215–30
- 395 [15] Rohlén R, Raikova R, Stålberg E and Grönlund C 2022 Estimation of contractile  
396 parameters of successive twitches in unfused tetanic contractions of single motor units – A  
397 proof-of-concept study using ultrafast ultrasound imaging in vivo *Journal of Electromyography*  
398 *and Kinesiology* **67** 102705
- 399 [16] Whittaker R G, Porcari P, Braz L, Williams T L, Schofield I S and Blamire A M  
400 2019 Functional magnetic resonance imaging of human motor unit fasciculation in amyotrophic  
401 lateral sclerosis *Annals of neurology* **85** 455–9

- 402 [17] Birkbeck M G, Blamire A M, Whittaker R G, Sayer A A and Dodds R M 2020  
403 The role of novel motor unit magnetic resonance imaging to investigate motor unit activity in  
404 ageing skeletal muscle *Journal of Cachexia, Sarcopenia and Muscle*
- 405 [18] Waasdorp R, Mugge W, Vos H J, De Groot J H, Verweij M D, De Jong N,  
406 Schouten A C and Daeichin V 2021 Combining ultrafast ultrasound and high-density EMG to  
407 assess local electromechanical muscle dynamics: A feasibility study *IEEE Access* **9** 45277–88
- 408 [19] Sierra González D and Castellini C 2013 A realistic implementation of  
409 ultrasound imaging as a human-machine interface for upper-limb amputees *Frontiers in*  
410 *neurorobotics* **7** 17
- 411 [20] Dhawan A S, Mukherjee B, Patwardhan S, Akhlaghi N, Diao G, Levay G, Holley  
412 R, Joiner W M, Harris-Love M and Sikdar S 2019 Proprioceptive sonomyographic control: A  
413 novel method for intuitive and proportional control of multiple degrees-of-freedom for  
414 individuals with upper extremity limb loss *Scientific reports* **9** 1–15
- 415 [21] Rohlén R, Antfolk C and Grönlund C 2022 Optimization and comparison of two  
416 methods for spike train estimation in an unfused tetanic contraction of low threshold motor  
417 units *Journal of Electromyography and Kinesiology* **67**
- 418 [22] Loupas T, Powers J T and Gill R W 1995 An axial velocity estimator for  
419 ultrasound blood flow imaging, based on a full evaluation of the Doppler equation by means of  
420 a two-dimensional autocorrelation approach *IEEE Transactions on Ultrasonics, Ferroelectrics,*  
421 *and Frequency Control* **42** 672–88
- 422 [23] Holobar A and Zazula D 2007 Multichannel blind source separation using  
423 convolution kernel compensation *IEEE Transactions on Signal Processing* **55** 4487–96
- 424 [24] Cerone G L, Giangrande A, Ghislieri M, Gazzoni M, Piitulainen H and Botter A  
425 2022 Design and validation of a wireless Body Sensor Network for integrated EEG and HD-  
426 sEMG acquisitions *IEEE Transactions on Neural Systems and Rehabilitation Engineering* **30**

- 427 61–71
- 428 [25] Cerone G L, Botter A and Gazzoni M 2019 A modular, smart, and wearable  
429 system for high density sEMG detection *IEEE Transactions on Biomedical Engineering* **66**  
430 3371–80
- 431 [26] Botter A, Vieira T M M, Loram I D, Merletti R and Hodson-Tole E F 2013 A  
432 novel system of electrodes transparent to ultrasound for simultaneous detection of myoelectric  
433 activity and B-mode ultrasound images of skeletal muscles *Journal of Applied Physiology* **115**  
434 1203–14
- 435 [27] Børstad T K 2013 DSPView *MATLAB Central File Exchange*
- 436 [28] Del Vecchio A, Holobar A, Falla D, Felici F, Enoka R M and Farina D 2020  
437 Tutorial: Analysis of motor unit discharge characteristics from high-density surface EMG  
438 signals *Journal of Electromyography and Kinesiology* **53** 102426
- 439 [29] Gallina A and Vieira T 2015 Territory and fiber orientation of vastus medialis  
440 motor units: a surface electromyography investigation *Muscle & Nerve* **52** 1057–65
- 441 [30] Stone J V, Porrill J, Porter N R and Wilkinson I D 2002 Spatiotemporal  
442 independent component analysis of event-related fMRI data using skewed probability density  
443 functions. *Neuroimage* **15** 407–21
- 444 [31] Farina D, Fattorini L, Felici F and Filligoi G 2002 Nonlinear surface EMG  
445 analysis to detect changes of motor unit conduction velocity and synchronization *J Appl Physiol*  
446 (1985) **93** 1753–63
- 447 [32] Stålberg E and Dioszeghy P 1991 Scanning EMG in normal muscle and in  
448 neuromuscular disorders *Electroencephalography and Clinical Neurophysiology/Evoked*  
449 *Potentials Section* **81** 403–16
- 450 [33] Botter A, Vieira T, Carbonaro M, Cerone G L and Hodson-Tole E F 2021  
451 Electrodes' Configuration Influences the Agreement Between Surface EMG and B-Mode

- 452    Ultrasound Detection of Motor Unit Fasciculation *IEEE Access* **9** 98110–20
- 453    [34]            Hyvärinen A, Karhunen J and Oja E 2001 *Independent Component Analysis*
- 454    (Wiley-Interscience)
- 455    [35]            Wakeling J M, Ross S A, Ryan D S, Bolsterlee B, Konno R, Domínguez S and
- 456    Nigam N 2020 The Energy of Muscle Contraction. I. Tissue Force and Deformation During
- 457    Fixed-End Contractions *Frontiers in Physiology* **11**
- 458    [36]            Herzog W 2017 Skeletal muscle mechanics: questions, problems and possible
- 459    solutions *J NeuroEngineering Rehabil* **14** 98
- 460    [37]            Rohlén R, Lundsberg J, Malesevic N and Antfolk C *A fast blind source*
- 461    *separation algorithm for decomposing ultrafast ultrasound images into spatiotemporal muscle*
- 462    *unit kinematics*

463

## 464    **Acknowledgements**

465    RR is supported by the Swedish Research Council for Sport Science (grant number: D2023-

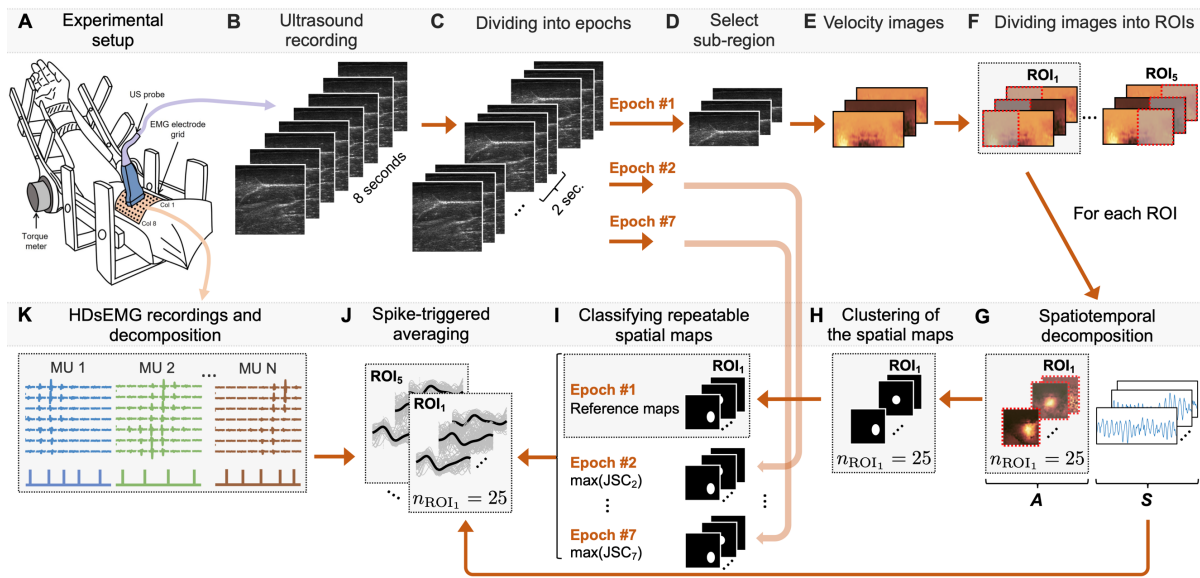
466    0003). MC is supported by the project “Trajector-AGE” (grant number: 2020477RW5PRIN),

467    funded by the Italian Ministry of Universities and Research. CG is supported by the Swedish

468    Research Council (grant number: 2022-04747).

469

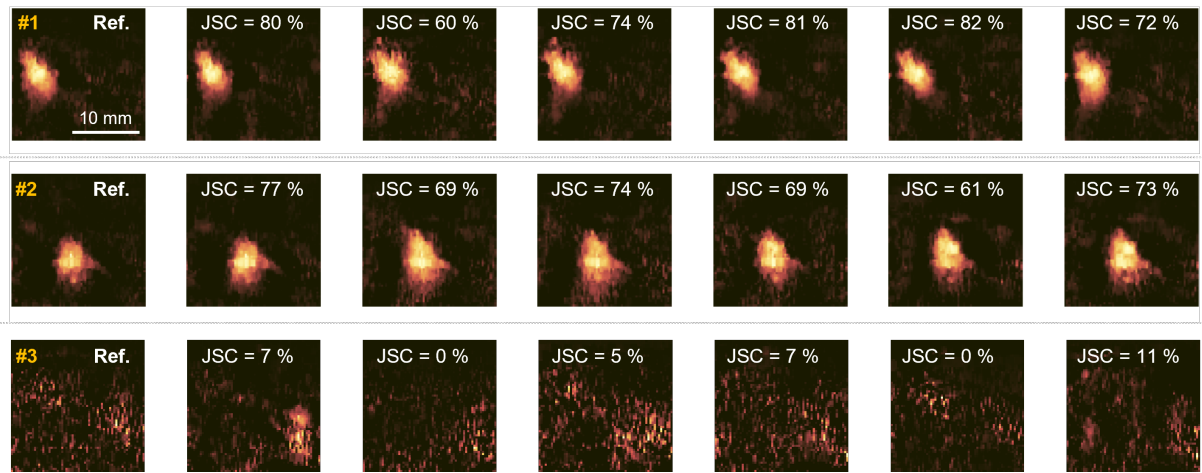
470 **Figures**



471

472 **Figure 1.** Illustration of the ultrasound data processing and identification of repeatable spatial maps. **A.**  
 473 Experimental setup with simultaneous ultrafast ultrasound (UUS) and high-density surface electromyography  
 474 (HDsEMG) recordings (adapted from Carbonaro et al. (2022) [6]). **B.** Eight-second recordings using UUS (40x40  
 475 mm, 2500 Hz) plane wave imaging. **C.** The recordings were divided into seven partially overlapping epochs of  
 476 two seconds each. **D.** A sub-region was selected within the HDsEMG detection volume (20x40 mm). **E.** Tissue  
 477 velocity images were estimated. **F.** The velocity images were divided into five region-of-interests (ROIs), i.e.,  
 478 20x20 mm each. **G.** Each ROI was decomposed into 25 components, i.e., 25 temporal signals ('S') and 25 spatial  
 479 maps ('A'). **H.** The spatial maps were clustered and processed to generate a binary map, with zeros being the  
 480 background and ones being the largest intensity of the territory. **I.** The binary maps were used for calculating the  
 481 Jaccard Similarity Coefficient (JSC) for each component in the epoch (second to the seventh) with the first epoch  
 482 as a reference. The maximal JSC was retained for each epoch, and then the mean JSC (based on the maximal JSC  
 483 for all epochs) was calculated. **J.** Then, spike-triggered averaging of the components' temporal signal was  
 484 performed using the motor unit (MU) spike trains instants from the **K.** HDsEMG decomposition.

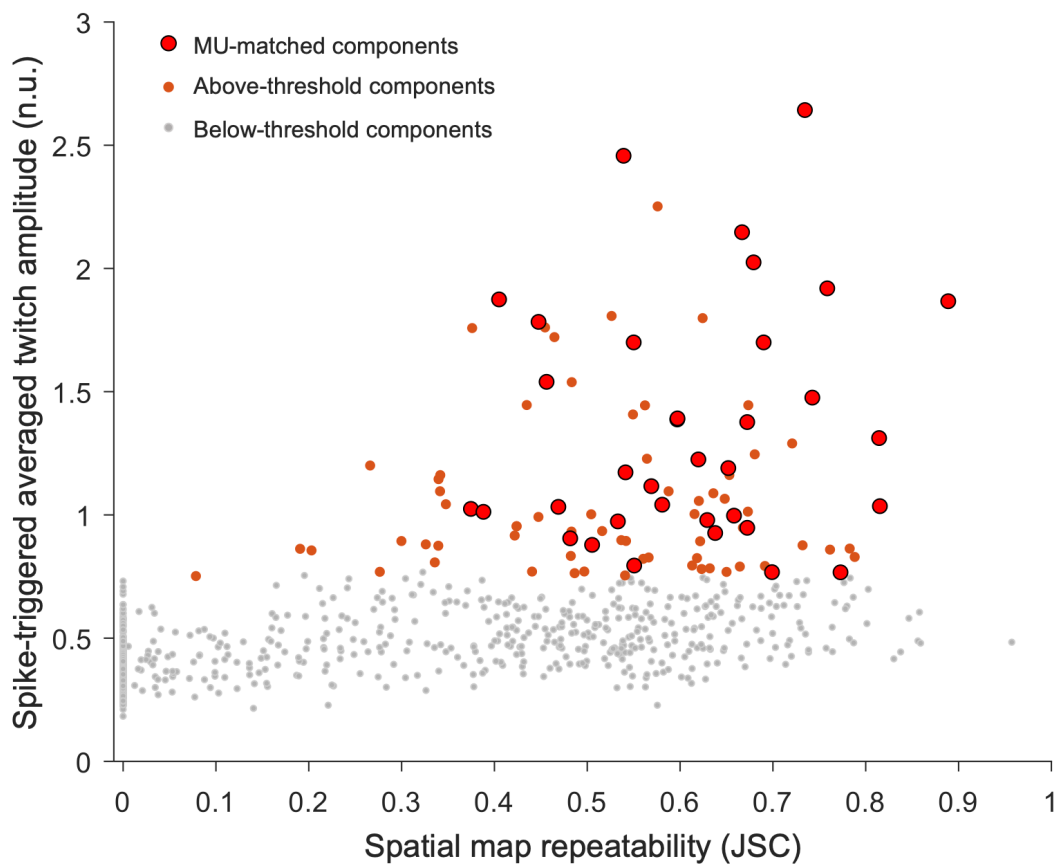
485



486

487 **Figure 2.** Examples of repeatable spatial maps from two repeatable components (#1 to #2) and one non-repeatable  
488 component (#3) of the same recording and region-of-interest (ROI) based on the Jaccard Similarity Coefficient  
489 (JSC). The first two-second epoch is the reference (defined as Ref).

490

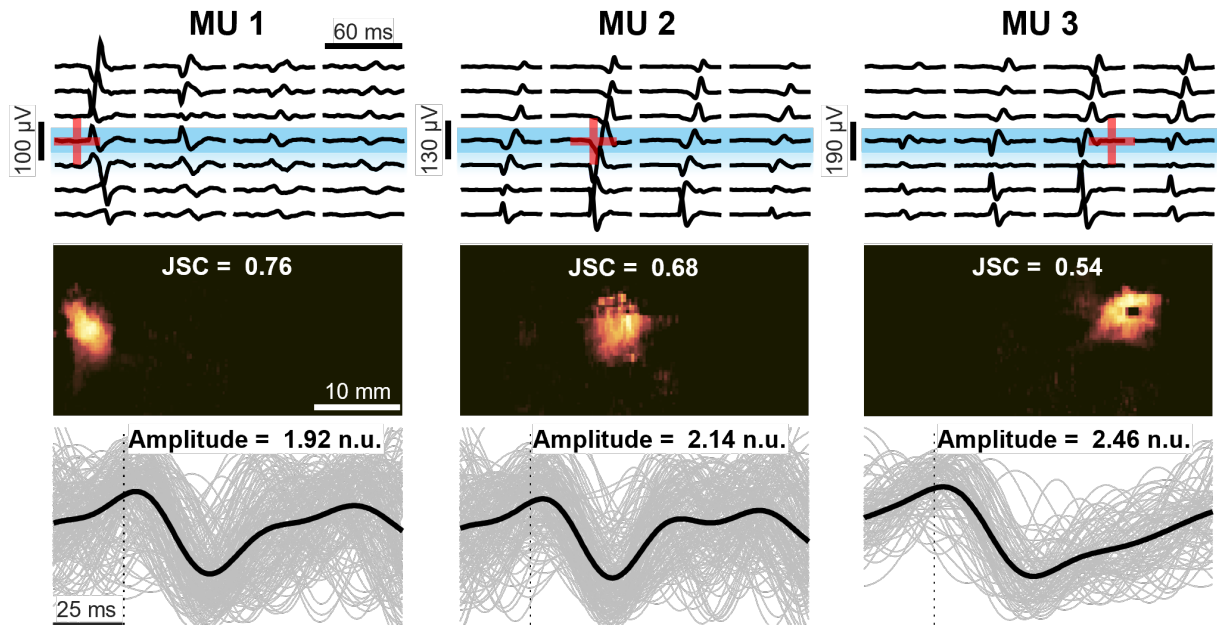


491

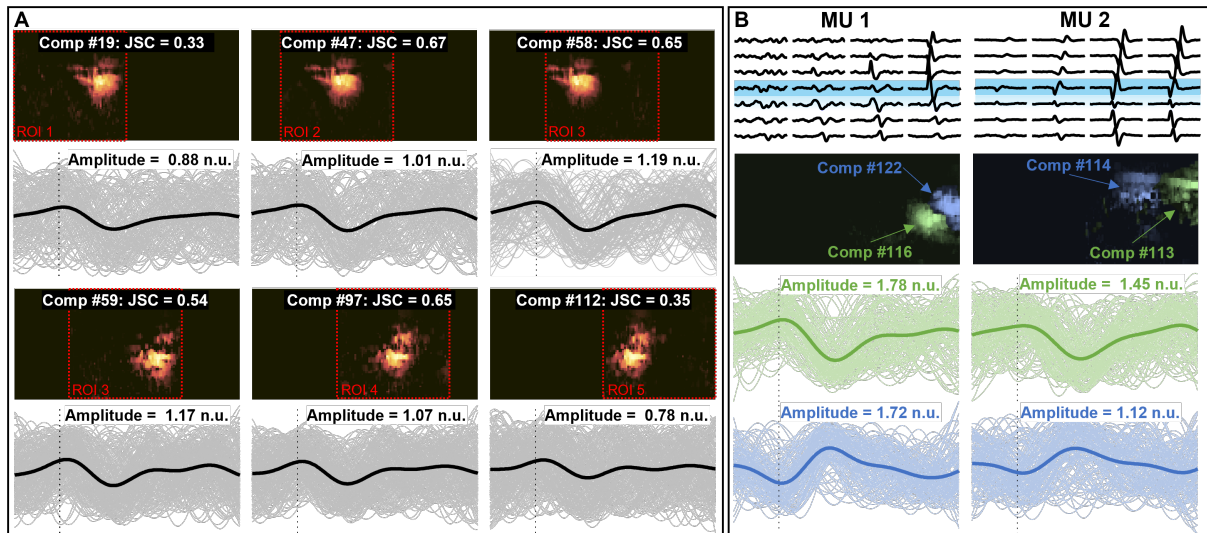
492 **Figure 3.** Relationship between Jaccard Similarity Coefficient (JSC) and putative twitches with the highest spike-  
493 triggered averaged twitch amplitude. Grey dots are the putative twitches below the noise threshold that were

494 discarded. The red circles correspond to the 35 MU-matched components. All the MU-matched components have  
495 JSC over 0.38 (i.e., repeatable). Orange dots refer to multiple components associated with the same MU (e.g.,  
496 twisting/split territory, duplicate components, etc., see Fig. 5).

497



499 **Figure 4.** Three representative matches between repeatable components and the motor units (MUs). The upper  
500 panels show the MU action potentials and the centroid of the EMG distribution (red '+'). In this representation,  
501 only the four columns of the EMG grid superimposed on the ultrasound probe (blue rectangle) are shown. The  
502 middle panels show the mean spatial map of the repeatable component and the corresponding mean JSC. Finally,  
503 lower panels depict the spike-triggered averaged velocity twitch (black line) based on the triggered signals from  
504 all seven epochs (grey lines) and the corresponding peak-to-peak amplitude. The vertical dotted lines corresponded  
505 to the firing instants of the MUs identified from HDsEMG decomposition and used for the triggering.



506

507 **Figure 5.** Examples of multiple components associated with the same MU. **A.** Two examples of three different  
508 components (belonging to different ROIs) with a similar spatial map (active region) matched with the same MUs.  
509 In this case, the three components were merged into the same repeatable component. **B.** Two examples of possible  
510 twisting MUs. The MUs were matched with two components showing active regions close to each other and the  
511 average twitches showing opposite profiles. Green twitches are negative (movements towards the probe/skin), and  
512 blue twitches, on the contrary, are positive (movements away from the probe/skin).

513



## 514 **Tables**

515 **Table 1.** Descriptive statistics about the motor unit-matched repeatable components.

<b>MU-matched repeatable components</b>	<b>N = 35</b>
Jaccard Similarity Coefficient, JSC	0.61 ± 0.13 (0.38; 0.89)
Amplitude (n.u)	1.35 ± 0.49 (0.76; 2.64)
Centroid-to-centroid (EMG-UUS) (mm)	5.35 ± 5.17 (0.01; 15.83)
Depth (mm)	9.47 ± 2.40 (2.90; 14.01)
Diameter (mm)	4.03 ± 1.28 (1.45; 7.25)
Area (mm <sup>2</sup> )	14.06 ± 8.71 (1.66; 41.30)

516 Mean ± SD (min; max), MU = motor unit, EMG = electromyography, UUS = ultrafast ultrasound, n.u. = normalised units.  
517